Simulations of the SLAC Plasma Lens Experiment

Shinichi Masuda* and Pisin Chen†

*Department of Physics and Astronomy, University of California, Los Angeles, CA 90024-1547
†Stanford Linear Accelerator Center, Stanford University, Stanford, CA 94309

Abstract. A plasma lens experiment is planned at SLAC with high energy electron beams and high plasma density. We have developed a PIC code, SPLASH (Simulation of Plasma Lens And Synchrotron-radiation in Hybrid), for computer simulations of this experiment. The plasma lens focusing effects are simulated for the beam energy at 30 and 50 GeV and the plasma density between $n_p/n_b = 0.1$ and 100. The original bunch size is 3 and 5 μm in radius. Due to plasma focusing, the beam size is reduced, which is progressively more effective when the relative plasma density increases from the "underdense"regime to the "overdense"one. However, field compensation due to the plasma return current renders the plasma focusing effect suppressed when the plasma density further increases to the "superdense"regime. The beam waist is located between ± 20 mm around the original focal point. In the most effective case, the beam is focused from 5 μm to 2 μm and from 3 μm to 1 μm.

INTRODUCTION

The effect of the plasma on the charged particle beam passing through it has been studied in recent years. The beam excites the electromagnetic waves in the plasma which affects the beam itself. The effects of the excited wave acting on the beam appear as the focusing and the acceleration. The plasma lens as a final focus device for future linear accelerators has been developed theoretically [1–6] and experimentally [7–9]. The experiments conducted in past demonstrated the plasma lens effect for the electron beam with the energy of several MeV and the plasma density of the order of 10^{10} to 10^{12}cm^{-3}.

For future linear colliders, there is need to investigate the plasma lens with the energy and the plasma density many order of magnitude higher than that in these proof of principle experiments. The E-150 SLAC plasma lens experiment is planned with the electron energy up to 50 GeV, the wide range of the plasma density and the beam density around $10^{18}\,\text{cm}^{-3}$ [10].

A PIC (Particle-In-Cell) code, *SPLASH* (Simulation of Plasma Lens And Synchrotron-radiation in Hybrid), was developed for computer simulations of this experiment. In this paper we report on the simulation model and the simulation results.

SIMULATION MODEL AND PARAMETERS

Our simulation code treats two dimensional axially symmetric system. The electromagnetic field and the current density on the r-z plane are calculated on each grid point by the axially symmetric Maxwell equations. Particle motion is calculated by the Lorentz force equation in the three dimensional Cartesian coordinates. Each macro particle has the shape like a ring. The current densities on each grid point are calculated by the volume weighting scheme in the r-z around the z-axis for the position and velocity of each particle projected on the r-z plane. The electromagnetic field acting on each macro particle is interpolated by the same weighting scheme. The quantities such as the electromagnetic field and the position and velocity of the particle are advanced in time by the leap-frog method.

Figure 1 shows the simulation model. The system is enclosed by a cylinderical conducting wall. A plasma column is located at the center of the system. An initially given electron bunch goes into the system as shown in Fig.1.

Following the convention in accelerator physics, we take a s-axis along the z-axis so that an original waist of the beam without plasma lens is located at $s = 0$. Position of the focused beam waist is represented by the s-axis in this paper.

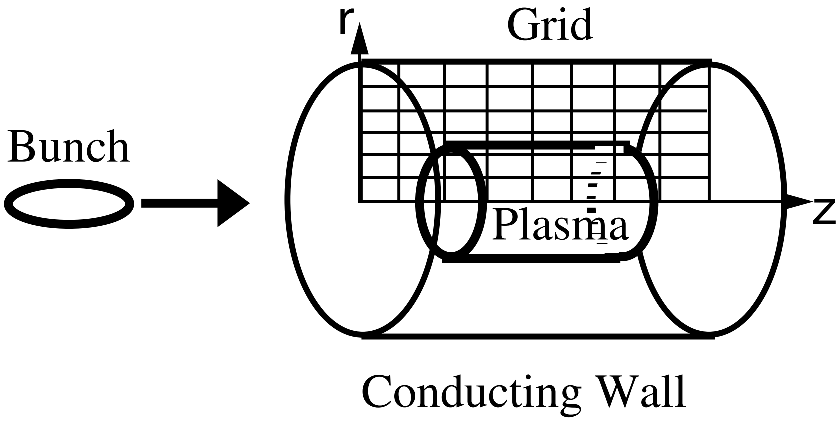

FIGURE 1. The simulation model for the plasma lens.

TABLE 1. Beam parameters in the SLAC plasma lens experiment.

Quantities	**Values**
Energy E	30 and 50 GeV
Population N	$1 \sim 4 \times 10^{10}$
Emittance ϵ_n	2 or 3×10^{-5} m rad
Bunch size σ^*_{r0}	$3 \sim 5\,\mu$m
Bunch length σ_z	$0.45 \sim 0.7$ mm
Density ratio n_p/n_{b0} [a]	$0.1 \sim 100$

[a] n_p and n_{b0} are the plasma and beam density at the lens entrance, respectively

Spatial distribution of the plasma column, in our case 3 mm in length and 30 μm in radius, is assumed to be uniform. The plasma lens entrance is located at $s = -20$ mm. Cold plasma is supposed, i.e., initial velocity of each plasma particle is zero because the thermal effect of the plasma is negligible due to small thermal velocity in our experiment.

The bunch comes into the system along the s-axis as shown in Fig.1. Initial distribution of the beam particles is assumed to be Gaussian for both of spatial and velocity distributions. The Gaussian distribution at the initial position, $s = s_0$, is

$$n_b(r,s) = n_{b0} \exp[-\frac{r^2}{2{\sigma^*_{r0}}^2(1+(s-s_0)^2/{\beta^*_0}^2)}] \exp[-\frac{(s-s_0)^2}{2\sigma_z^2}] \tag{1}$$

where n_{b0} is the density at center of the beam, β^*_0 and σ^*_{r0} is the beta function and the rms size at the original beam waist, respectively, σ_z is the rms bunch length. Beam parameters are shown in Table 1.

In this simulation changes in the beam size along the beam line are calculated to obtain some information for real measurements. The beam particles are tracked after they pass through the plasma lens. Intersections of each particle orbit on the x-y planes, which are located on the s-axis along the beam line, are collected. Then the *rms* and the *hwhm* (half with half maximum) sizes are calculated from the time integrated distributions of the points of intersections on each plane. We will discuss the simulation results in next section.

SIMULATION RESULTS AND DISCUSSION

Characteristics of Plasma Focused Beam

The plasma lens works differently from the conventional lens using magnetic fields because the intensity of the excited wakefield changes along the bunch. Then, the

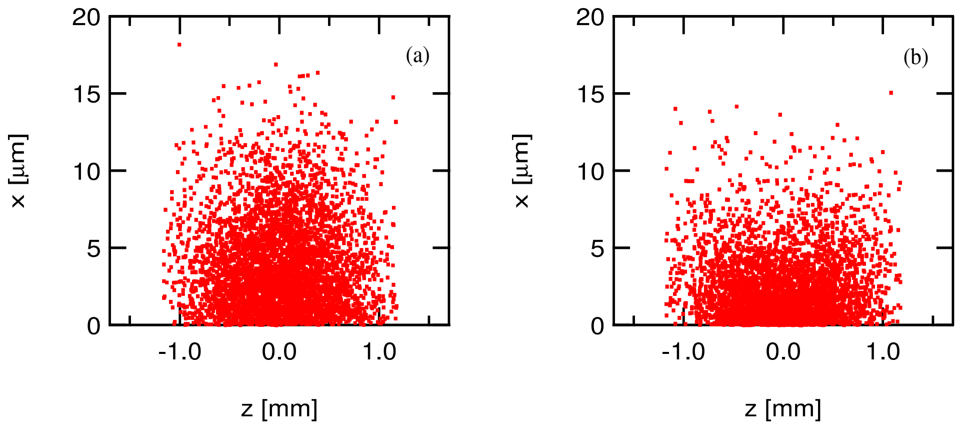

FIGURE 2. Snap shots of the bunch. Positions of each particle in the bunch projected on x-z plane are plotted. Only upper half of x-z distribution is shown because lower half of the distribution is symmetric. The beam parameters are $E = 46\,\mathrm{GeV}$, $N = 2 \times 10^{10}$, $\epsilon_n = 3 \times 10^{-5}\,\mathrm{mrad}$, $\sigma^*_{r0} = 4.74\,\mu\mathrm{m}$ and $\sigma_z = 0.47\,\mathrm{mm}$, $n_p = 20 \times 10^{16}\,\mathrm{cm}^{-3}$. (a) shows plots of the particles in the bunch at the plasma lens entrance. (b) Snap shot for the bunch near the focal point.

focusing strength is different for different z-position in the bunch. Snap shots of the beam at different time are shown in Fig.2. The initial profile of the beam at the lens entrance is Gaussian (see Fig.2(a)). Figure 2(b) shows the bunch near the focal point. It is seen that the focusing effect is strongest around the center of the bunch. Because of this, we expect that the radial profile of the bunch at the focal point deviates from the Gaussian distribution.

The evolution of the beam envelope along the beam line downstream of the plasma lens is shown in Fig.3. The beam size is determined by two different ways, the rms and the hwhm. When without plasma lens, the envelopes calculated by both rms and hwhm sizes evolve much the same way. This indicates that the radial profile does not much change along the beam line in this case. On the contrary, when the plasma is turned on the beam rms and hwhm sizes evolve differently. The focal length deduced from the hwhm envelope tends to the much shorter than that calculated by the rms size.

Changes of the radial profile along the beam line for the same beam parameters as that in Fig.3 are shown in Fig.4. Figure 5 shows phase space plots along the beam line with the same parameters. The divergence angle of the focused beam changes from $85\,\mu$rad to $200\,\mu$rad in this case. It is seen from Fig.5(a) that the focusing effect is strongest at $r(= \sqrt{x^2+y^2}) \sim 5\,\mu$m and is small at peripheral of the bunch. This is because the self-focusing plasma wakefield increases linearly with r for $r \ll \sigma_r$ and reaches a maximum at $r \approx 1.6 \times \sigma_r$. Then it decreases for $r > 1.6 \times \sigma_r$ as described by the equation for the overdense regime [1],

$$F_r(r) = k_p^2 \left\{ \int_{-\infty}^{r} r'dr' \, \exp(-\frac{r'^2}{2\sigma_r^2}) K_1(k_p r) I_0(k_p r') - \int_{r}^{\infty} r'dr' \, \exp(-\frac{r'^2}{2\sigma_r^2}) I_1(k_p r) K_0(k_p r') \right\}, \tag{2}$$

where k_p is the wave number of the plasma oscillation, K_n and I_m are the modified Bessel's functions.

Deviation of the radial profile from the Gaussian profile is small for the bunch just leaving the plasma lens (see Fig.4(a)). However, the profile becomes spiky near the beam waist further as shown in Fig.4(b) and (c). Figure 5 shows that the phase space ellipse rotates clockwise along the beam line. Strongly accelerated particles at $r \sim 1.6 \times \sigma_r$ (Fig.5(a)) concentrate to the core of the bunch when the bunch reaches the focal point as shown in Fig.5(b).

Such spiky distribution can be attributed to the dynamical nature of the plasma focusing in the overdense regime, where particles near the head and tail of the beam tend to receive a weaker focusing. In addition, nonlinear r-dependence of self-focusing field also contributes to this spiky distribution as mentioned above.

Dependence on Beam Energy and Density

SLAC E-150 experiment will be conducted with a wide range of the plasma density between $n_p/n_b = 0.1 \sim 100$. We obtained results from simulations for several plasma densities. Figure 6 shows the beam envelopes calculated by the hwhm for three different ratios of the plasma density to the beam density. For the

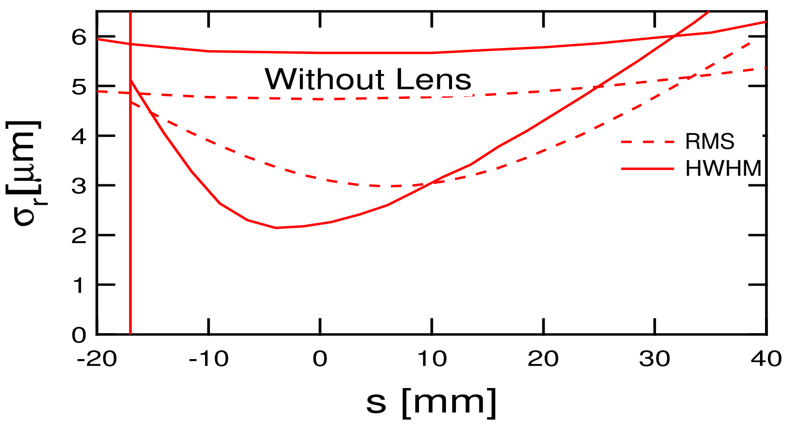

FIGURE 3. Comparison between the rms size and hwhm size of the bunch along the beam line. Original waist of the beam without lens is located at $s = 0$. The plasma lens entrance and exit are at $s = -20$ mm and $s = -17$ mm, respectively. The beam parameters are $E = 46$ GeV, $N = 2 \times 10^{10}$, $\epsilon_n = 3 \times 10^{-5}$ mrad, $\sigma_{r0}^* = 4.74\,\mu$m and $\sigma_z = 0.47$ mm, $n_p = 20 \times 10^{16}\,\mathrm{cm}^{-3}$.

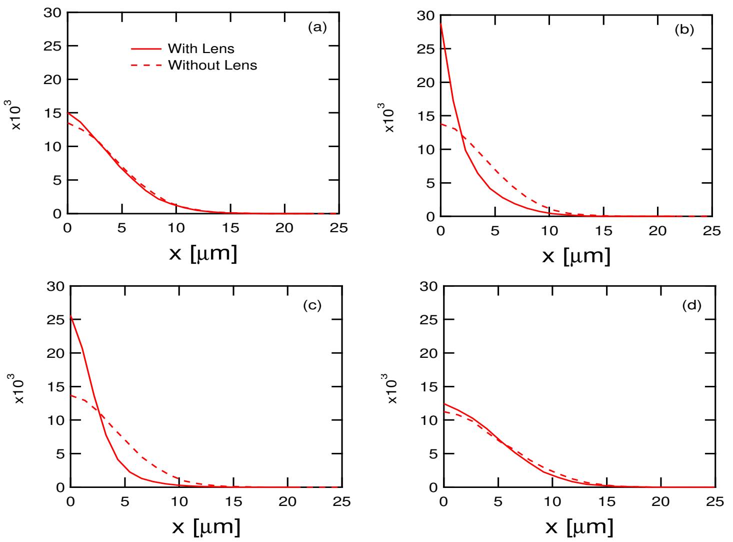

FIGURE 4. Radial profile of the bunch. Dashed curve indicates the radial profile of the original beam (without lens case). Solid curve is the radial profile when the plasma is turned on. The beam parameters are the same with those in Fig.3. (a) At the plasma lens exit, $s = -17$ mm. (b) At the beam waist calculated by the hwhm size, $s = -4$ mm. (c) At the beam waist calculated by the rms size, $s = 8$ mm. (d) On downstream away from the plasma lens, $s = 40$ mm.

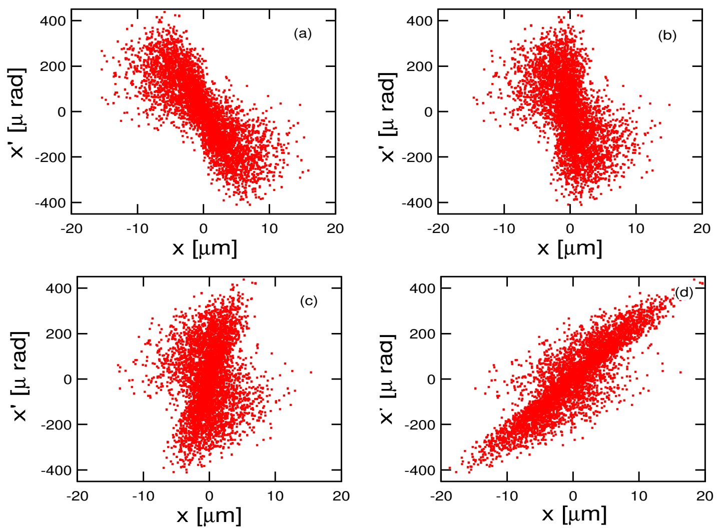

FIGURE 5. Phase space plots along the beam line. The beam parameters are the same with those in Fig.3. (a) At $s = -17$ mm. (b) At $s = -4$ mm. (c) At $s = 8$ mm. (d) At $s = 40$ mm.

underdense regime of $n_p/n_b = 0.3$, the beam waist moves to downstream of the original waist. On the contrary, the beam waist for the overdense case is located on upstream of the original waist. We found that the focusing effect is strongest

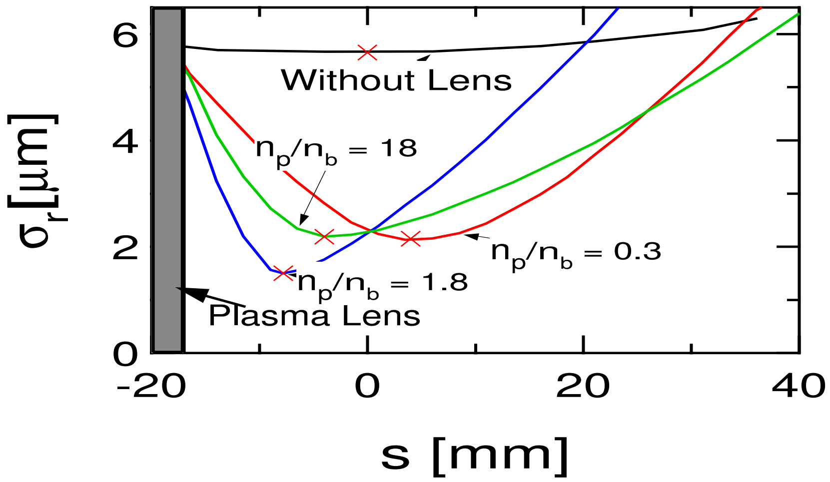

FIGURE 6. Beam envelopes for three different plasma densities, underdense ($n_p/n_{b0} = 0.3$), overdense ($n_p/n_{b0} = 1.8$) and superdense ($n_p/n_{b0} = 18$). Beam parameters are $E = 30\,\mathrm{GeV}$, $N = 2 \times 10^{10}$, $\epsilon_n = 3 \times 10^{-5}\,\mathrm{mrad}$, $\sigma^*_{r0} = 4.74\,\mu\mathrm{m}$ and $\sigma_z = 0.47\,\mathrm{mm}$. Cross symbols mark the focal point for each beams.

when $n_p/n_b = 1.8$. An incoming beam with $\sigma^*_{r0} \sim 5\,\mu\mathrm{m}$ is focused to $1.5\,\mu\mathrm{m}$ at the beam waist as shown in Fig.6.

Dependence of the focusing effect on the plasma density is shown in Fig.7. Po-

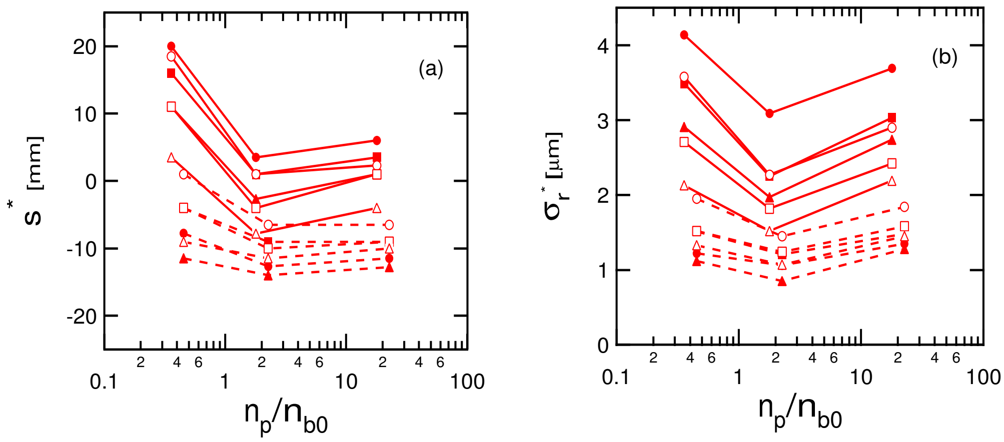

FIGURE 7. Dependency on density ratio. (a) Positions of the beam waist and (b) the beam sizes (hwhm) at the focal points are plotted versus the ratio of the plasma density to the density of the beam bunch. The beam parameters are $E = 30\,\mathrm{GeV}$ (open symbols), $E = 46\,\mathrm{GeV}$ (solid symbols), $N = 1\times10^{10}$ (circles), $N = 1.5\times10^{10}$ (squares), $N = 2\times10^{10}$ (triangles), $\sigma^*_{r0} = 4.74\,\mu\mathrm{m}$ (solid curves) $\sigma^*_{r0} = 3\,\mu\mathrm{m}$ (dashed curves) and $\sigma_z = 0.47\,\mathrm{mm}$.

sitions of the focal points are shown in Fig.7(a) and the beam sizes at the focal points are shown in Fig.7(b). For the underdense regime the beam waist moves closer to the plasma lens with an increase in the density ratio of the plasma to the beam. Then the focal length decreases with the density ratio. When the plasma density exceeds the beam density, the focal length increases for $5\,\mu$m incoming beam with the increase in the plasma density. The beam size decreases for the underdense regime and increases for the overdense regime with the increase of the plasma density.

Figure 7 shows also the energy dependence indicated by open symbols (30 GeV) and solid symbols (46 GeV). For the incoming beam of $5\,\mu$m in radius (solid curves) the focal length and the waist size at the energy of 46 GeV larger than that at the energy of 30 GeV. The focusing strength decreases with an increase in the energy in this case. However this dependence is opposite for case of $3\,\mu$m beam (dashed curves).

Circles, squares and triangles in Fig.7 indicate the results for the particle populations within the bunch, 1.0×10^{10}, 1.5×10^{10} and 2.0×10^{10}, respectively. It is seen that the focusing strength increases with an increase in the particle population for both of $3\,\mu$m and $5\,\mu$m beams.

Focusing of Positron Beams

For an eventual application of the plasma lens to high energy linear colliders, we are also interested in the plasma focusing of a positron beam. The theory [1]

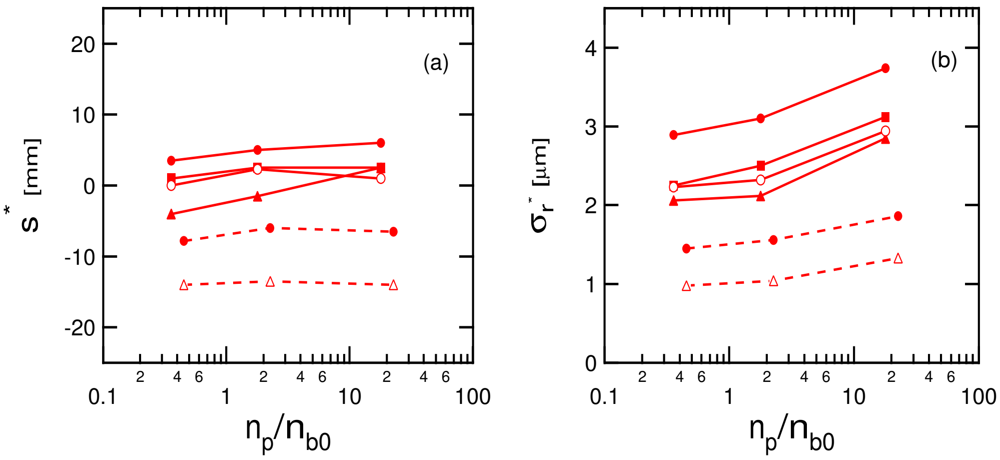

FIGURE 8. Focusing effect of the plasma lens for the positron beam case. (a) Position of the beam waist and (b) the beam size at the waist. The beam parameters are $E = 30$ GeV (open symbols), $E = 46$ GeV (solid symbols), $N = 1 \times 10^{10}$ (circles), $N = 1.5 \times 10^{10}$ (squares), $N = 2 \times 10^{10}$ (triangles), $\sigma^*_{r0} = 4.74\,\mu$m (solid curves) $\sigma^*_{r0} = 3\,\mu$m (dashed curves) and $\sigma_z = 0.47$ mm.

predicts that the focusing effect on the positron beam is the same as the electron case in the overdense regime.

We have performed the plasma lens simulations for the positron beams. The beam parameters are the same as those for the electron bunch. Figure 8 shows the focusing effect for the positron case. Dependency on the plasma density for the overdense regime shows good agreement with the electron case (see Fig.7 also) as expected by the theory. In the underdense regime, contrary to the electron case, the waist size increases with the increase of the plasma density. In addition, it is seen that the focusing strength of the underdense regime is stronger for the positron bunch than for the electron bunch.

Other characteristics of positron focusing, such as the dependencies on the energy and the population of the particle, are the same as those for the electron beam. The focusing strength decreases with the beam energy. The focused beam size as well as the focal length is inversely proportional to the beam density.

Simulation of Synchrotron Radiation

The plasma lens strongly deflects the particle orbit in the beam and would induce *SR* (synchrotron radiation). Experimentally, these SR photons induced by the plasma focusing provide a direct information on the plasma focusing strength. The E-150 experiment intends to construct a SR monitor for this purpose.

Computer simulation on this process is therefore important for the design of such an apparatus. The synchrotron radiation based on the quantum mechanical formulation [11] is included in our simulation code. An algorithm to handle dis-

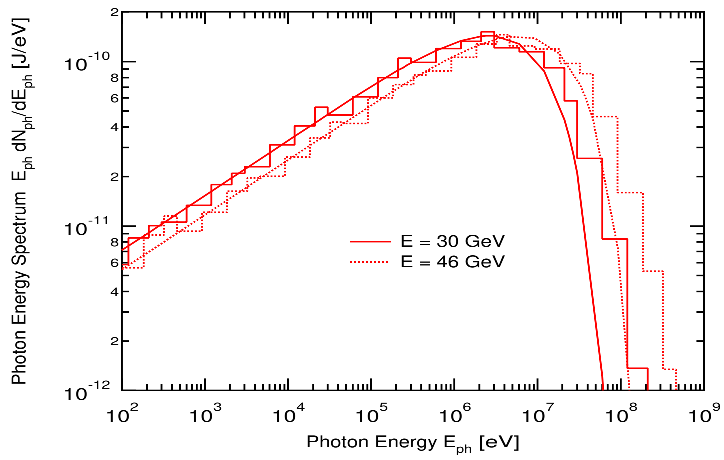

FIGURE 9. Energy spectra of photons emitted from electron bunch with energy of 30 GeV (solid) and of 46 GeV (dashed) during it passing through the plasma lens. Histograms show results from the simulations. Theoretical curves are also plotted. Beam parameters are $N = 2 \times 10^{10}$, $\sigma^*_{r0} = 5\,\mu$m and $\sigma_z = 0.65$ mm. The plasma density is 20×10^{16}cm^{-3} ($n_p/n_b \sim 2$).

crete photon emission is implemented following the technique in the code, DRNO [12]. Number of photons emitted from an electron during one simulation cycle can be calculated by $N_{ph}\Delta t$, where $N_{ph} = \int_0^{\hbar\omega_{\max}}[dN_{ph}(\hbar\omega)/d(\hbar\omega)]d(\hbar\omega)$ is the photon emission rate from an electron and Δt is the time step in the simulation. $N_{ph}\Delta t$, which is much smaller than unity, is proportional to the probability of the photon emission during the Δt. To simulate the discrete photon emission, a number provided by the uniform random number generator, which has value between $0 \sim 1$, is compared with $N_{ph}\Delta t$. When the number is smaller than $N_{ph}\Delta t$, the algorithm decides that a photon is emitted. The emitted photon energy is determined randomly according to the photon number spectrum, $dN_{ph}(\hbar\omega)/d(\hbar\omega)$; A uniform random number $(0 \sim 1)$ is provided as the argument of the inverse function of the accumulated spectrum, $\int_0^{\hbar\omega}[dN_{ph}(\hbar\omega')/d(\hbar\omega)']d(\hbar\omega)'/N_{ph}$. Then the photon energy, $\hbar\omega$, can be calculated from the inverse function. This inverse function works as a random number generator providing the photon number spectrum.

Figure 9 shows energy spectra of the photon emitted from the electron bunch. Histograms of energy spectra are plotted for the beams with energy of 30 GeV (solid) and of 46 GeV (dashed). Shapes of both spectra are similar as expected. Since the initial beam sizes of the 30 GeV and 46 GeV beams are the same and the plasma density was also the same, we expect that the SR critical frequencies in the two cases differ by the ratio of the beam energies.

To obtain the magnitude of the equivalent magnetic field for the plasma focusing, a theoretical intensity, $\hbar\omega[dN_{ph}/d(\hbar\omega)]N\Delta t_f$, was calculated, where $\Delta t_f \sim 10^{-11}$ sec is the flight time of the electron bunch passing through the lens, to fit the simulation results. The equivalent focusing field gradient was found to be $B/\sigma_r \sim 2.6 \times 10^8$ Gauss/cm for both 30 GeV and 46 GeV cases. This is to be compared with the theoretical prediction from the focusing strength of plasma lens [10], $K = 2\pi r_e n_b/\gamma$, where r_e is the classical electron radius and γ is the relativistic kinetic energy factor of the beam. The equivalent focusing field gradient is calculated as $B/\sigma_r \approx KE/e \sim 1.6 \times 10^8$ Gauss/cm. The simulation result and the theoretical prediction are reasonably agreed.

SUMMARY

We reported the results from the PIC simulations for the plasma lens experiment. The results indicate that the electron bunches of $3\,\mu$m and $5\,\mu$m are focused down to $1\,\mu$m and $2\,\mu$m, respectively. We confirm that the focusing strength varies from the underdense regime to the overdense regime, and the superdense regime, in agreement with the theoretical prediction. The electron bunch is strongly focused around $n_p/n_b \approx 1 \sim 2$. Table 2 summaries our simulation results relevant to the E-150 experiment.

We have also shown that the synchrotron radiation algorithm in our code appears to produce the correct physics, although further studies is needed before we can fully utilize it to assist the design of a synchrotron radiation monitor.

TABLE 2. Simulation results. ($\sigma_{r0}^{*} = 5\,\mu$m, $\sigma_z = 0.65\,$mm.)

Population N	**Density** n_p/n_b	**Waist** s^* [mm]	**Size** σ_r^* [μm]	**Divergence** [μrad]
$E = 29.6\,$GeV				
	0.3	9.35	3.42	125
1.0×10^{10}	1.8	4.30	2.93	135
	18	5.98	3.39	108
	0.3	2.62	2.27	205
2.0×10^{10}	1.8	-1.86	2.05	220
	18	-0.18	2.70	143
	0.3	-6.35	1.48	374
4.0×10^{10}	1.8	-10.3	1.51	382
	18	-7.47	2.08	207
$E = 46.0\,$GeV				
	0.3	13.8	4.19	104
1.0×10^{10}	1.8	12.2	3.45	107
	18	9.34	4.04	91
	0.3	8.79	2.99	148
2.0×10^{10}	1.8	2.62	2.53	156
	18	2.06	3.38	110
	0.3	-1.30	1.95	259
4.0×10^{10}	1.8	-6.91	1.84	267
	18	-2.98	2.49	146

ACKNOWLEDGMENTS

We deeply appreciate the helpful discussion and kind assistance from R. J. Noble, who lent us the SR code, DRNO.

REFERENCES

1. Chen P., *Part. Accel.* **20**, 171 (1987).
2. Chen P., *et. al.*, *IEEE Trans. Plasma Sci.* **15**, 218 (1987).
3. Rosenzweig J. B., *et. al*, *Phys. Rev. D* **39**, 2039 (1989).
4. Chen P., *et. al.*, *Phys. Rev. D* **40**, 923 (1989).
5. Su J.J., *et. al.*, *Phys. Rev. A* **41**, 3321 (1990).
6. Chen P., *Phys. Rev. A* **45**, R3398 (1992)
7. Rosenzweig J. B., *et. al.*, *Phys. Rev. Lett.* **61**, 98 (1988).
8. Nakanishi H., *et. al.*, *Phys. Rev. Lett.* **66**, 1870 (1991).
9. Hairapetian G., *et. al.*, *Phys. Rev. Lett.* **72** 2403 (1994).
10. Chen P., *et. al.*, "SLAC Proposal E-150", SLAC (1997);
    Chattopadhyay S., *et. al.*, Wkshp. Adv. Accel. Concepts, 1998.
11. Sokolov A. A, and Ternov I. M., *Synchrotron Radiation*, Pergamon, Berlin, 1968.
12. Noble R. J., *Nucl. Inst. Meth.* **A256**, 427 (1987).